Creating and manipulating entangled optical qubits in the frequency domain

Laurent Olislager,[1,*] Erik Woodhead,[2] Kien Phan Huy,[3] Jean-Marc Merolla,[3] Philippe Emplit,[1] and Serge Massar[2]
[1]*OPERA–Photonique, CP 194/5, Université libre de Bruxelles, avenue F.D. Roosevelt 50, Brussels B-1050, Belgium*
[2]*Laboratoire d'Information Quantique, CP 225, Université libre de Bruxelles, avenue F.D. Roosevelt 50, Brussels B-1050, Belgium*
[3]*Département d'Optique P. M. Duffieux, Institut FEMTO–ST, Unité Mixte de Recherche du CNRS 6174, Université de Franche-Comté, route de Gray 16, Besançon F-25030, France*
(Received 4 March 2014; published 22 May 2014)

Radio-frequency phase modulation of frequency-entangled photons leads to a two-photon interference pattern in the frequency domain. In recent experiments, the pattern was measured with narrow-band frequency filters which select photons belonging to a given frequency bin. Here we show how photons can be grouped into even and odd frequencies by using periodic frequency filters called interleavers. In our theoretical analysis we show how this reduces the high-dimensional photon state to an effective two-dimensional state. This is of interest for applications such as quantum cryptography or low-dimensional tests of quantum nonlocality. We then report an experimental realization of this proposal. The observed two-photon interference pattern and violation of the CHSH inequality—the simplest binary-outcome Bell inequality—are in good agreement with the theoretical predictions.

DOI: 10.1103/PhysRevA.89.052323 PACS number(s): 42.50.Ex, 03.67.Hk

I. INTRODUCTION

Entangled photons are a key resource for quantum information processing and communication. During past decades, all degrees of freedom of photons have been used for entanglement experiments, including polarization [1–3], position and momentum [4], angular momentum [5], and time-energy [6–11]. The latter degree of freedom is particularly interesting for long-distance quantum communication, as it propagates essentially undisturbed through optical fibers over large distances. Most experiments exploited the concept of *time bins* originally proposed in Refs. [12,13], in which the photons are detected at discrete times. Recently we have introduced the concept of *frequency bins*, in which the photons are detected within discrete frequency intervals [14,15]. The latter works are based on earlier works in which the frequency degree of freedom was used to code information in attenuated coherent pulses for quantum key distribution applications [16–18]. Phase modulation of quantum light has also been studied in, e.g., Refs. [19–21].

The advantages of frequency-bin entanglement are that it can be manipulated and measured using standard telecommunication components such as electro-optic phase modulators and narrow-band fiber Bragg gratings, that raw visibilities in excess of 99% can readily be obtained (comparable to the highest visibilities obtained using other photonic degrees of freedom), that high-dimensional quantum states can be manipulated (dimension as high as 11 easily obtained), and that no interferometric stabilization is required over laboratory distance scales (meters of optical fibers).

In the experiments [14,15], electro-optic phase modulators generated a high-dimensional frequency interference pattern which was observed with narrow-band frequency filters, each selecting a given frequency bin. While the high dimensionality of the entangled state can be beneficial in some quantum information applications, it is sometimes desirable to work with well-known two-dimensional states for which most quantum communication protocols, such as the BB84 key distribution scheme [22], are designed. In addition, when the states are two dimensional, it is easier to access all measurement outcomes simultaneously since only four detectors are needed, which is better suited for tests of the CHSH Bell inequality [23]. (By contrast, in our earlier work [14,15], the reported violation of the CH74 inequality [24] on a higher-dimensional frequency entangled state was based on a simplifying assumption on the marginal statistics that was not tested directly.) The CHSH inequality is the standard and simplest inequality to use when checking for violation of local causality. It has been used for instance in experiments involving photons [2–4,9], trapped ions [25], and superconducting qubits [26]. It is also the basis for some of the most important potential applications of nonlocality, such as device-independent key distribution [27] and randomness expansion [28].

Here we show how to define, manipulate, and measure effective two-dimensional states in the frequency domain. The key idea is to use as measurement device a periodic filter that selects two sets of frequency bins, those with *even* and *odd* frequencies respectively. This implements a coarse-grained measurement that projects onto two orthogonal subspaces. Such periodic frequency filters are standard components in the telecommunication industry, known as *interleavers*. With this approach, we observe a two-dimensional two-photon interference in the frequency domain and violation of the CHSH Bell inequality [23]. This is realized by simultaneously measuring all coincidence probabilities (no further assumption is needed for the Bell test, contrary to Refs. [14,15]).

A further interest of the present approach is that it allows one in principle to manipulate and measure frequency-entangled photons that are produced by a broadband source with low spectral brightness, as the interleavers that separate the even and odd frequencies act over a very broad bandwidth. This, however, requires dispersion compensation, as otherwise photons with different detunings exhibit different interference patterns that average to zero over the bandwidth of the photons.

*lolislag@ulb.ac.be

The paper is divided into two main parts. In the first part we describe theoretically how effective qubits corresponding to even and odd frequencies can be introduced and how electro-optic phase modulators realize rotations in this two-dimensional space. We compute how the two-photon correlations depend on the amplitude and phase of the radio-frequency signals driving the phase modulators. From these expressions we show that the maximum possible violation of the CHSH inequality is 2.566. In the second part we describe our experimental setup. We report two-photon interference patterns in good agreement with the theoretical predictions and report a violation of the CHSH inequality of 2.334 ± 0.008. The reader principally interested in the experiment may skip directly to Sec. IV.

II. OUTLINE OF THE EXPERIMENT

Our experiment is schematized in Fig. 1. It is based on three components that we briefly describe:

(1) A source S produces the frequency-entangled state

$$|\Psi\rangle = \int d\omega\, f(\omega)|\omega_0+\omega\rangle|\omega_0-\omega\rangle \simeq \int d\omega|\omega_0+\omega\rangle|\omega_0-\omega\rangle, \quad (1)$$

where $f(\omega)$ characterizes the two-photon bandwidth. Because f varies slowly with frequency, for the theoretical analysis it is often useful to approximate it as constant as in the second line.

(2) A phase modulator driven by a radio-frequency signal $v\cos(\Omega t-\gamma)$ with adjustable amplitude v and phase γ realizes the unitary transformation

$$|\omega\rangle \mapsto \sum_{p\in\mathbb{Z}} J_p(c)e^{ip(\gamma-\pi/2)}|\omega+p\Omega\rangle, \quad (2)$$

$J_p(c)$ being the pth-order Bessel function of the first kind, with normalized amplitude $c=\pi v/V_\pi$ where V_π characterizes the response of the modulator.

(3) An interleaver is a component used in the telecommunication industry that separates the frequencies centered on $\omega_0+2n\Omega$ from those centered on $\omega_0+(2n+1)\Omega$, where ω_0 is a fixed offset, and $n\in\mathbb{Z}$. We use interleavers as components that allow the measurement of even and odd frequencies. If we follow the interleaver by single-photon detectors, then a click of one of the detectors corresponds to the projection onto one

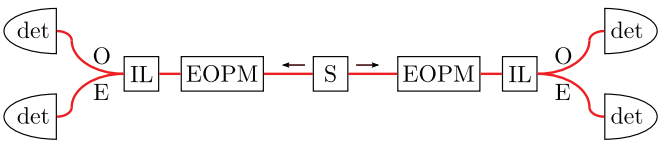

FIG. 1. (Color online) Simple schematic of the experiment. The source (S) produces frequency-entangled photons. Two electro-optic phase modulators (EOPM) driven by radio-frequency signals with identical frequency Ω but different amplitudes and phases, (a,α) and (b,β), realize interference in the frequency domain. Interleavers (IL) send the even (E) and odd (O) frequency bins to separate single-photon detectors (det).

of the two operators:

$$\Pi_{\rm E} = \int_{-\Omega}^{+\Omega} d\omega\, g(\omega)\sum_n \Pi_{\omega_0+\omega+2n\Omega}, \quad (3)$$

$$\Pi_{\rm O} = \int_{-\Omega}^{+\Omega} d\omega\, g(\omega)\sum_n \Pi_{\omega_0+\omega+(2n+1)\Omega}, \quad (4)$$

where $\Pi_\omega = |\omega\rangle\langle\omega|$ is the projector onto the frequency state $|\omega\rangle$ and $g(\omega)$ is a function characteristic of the interleaver which is maximal in the vicinity of $\omega=0$ and very small when $|\omega|>\Omega/2$. Examples of transmission spectra of interleavers can be found in Fig. 2.

The experiment consists of preparing the state, sending Alice's and Bob's photons through phase modulators driven by radio-frequency signals with identical frequency Ω but different amplitudes and phases, (a,α) and (b,β), and finally determining whether the frequency is even or odd by passing the photon through interleavers and then sending the output to single-photon detectors.

III. THEORETICAL ANALYSIS

A. Discrete and offset space

Because the phase modulator shifts the frequency by Ω and the interleaver is sensitive only to frequency modulo 2Ω, it is convenient to rewrite the state as

$$\begin{aligned}|\Psi\rangle &= \int_{-\Omega/2}^{+\Omega/2} d\omega \sum_{n=-\infty}^{+\infty} f(\omega+n\Omega) \times |\omega_0+\omega+n\Omega\rangle|\omega_0-\omega-n\Omega\rangle \\ &\simeq \int_{-\Omega/2}^{+\Omega/2} d\omega \sum_{n=-\infty}^{+\infty} f_n|n,\omega\rangle|-n,-\omega\rangle \\ &= \sum_{n\in\mathbb{Z}} f_n|n\rangle|-n\rangle\otimes\int_{-\Omega/2}^{\Omega/2} d\omega|\omega\rangle|-\omega\rangle \\ &= |\Psi_\Pi\rangle\otimes|\Psi_{\rm off}\rangle, \end{aligned} \quad (5)$$

where we suppose that f varies slowly so that we can neglect the dependence on ω: $f(\omega+n\Omega)\simeq f_n$. The identification $|n\rangle\otimes|\omega\rangle = |n,\omega\rangle = |\omega_0+n\Omega+\omega\rangle$ defines a factorization $\mathcal{H}_{\rm F}=\mathcal{H}_\Pi\otimes\mathcal{H}_{\rm off}$ of the Hilbert space $\mathcal{H}_{\rm F}$ of frequency states into separate "discrete" and "offset" spaces, $\mathcal{H}_\Pi$ and $\mathcal{H}_{\rm off}$, respectively, with respect to which the source state $|\Psi\rangle$ is (approximately) separable. We adopt the normalization

$$\langle m|n\rangle = \delta_{mn}, \quad (6)$$

$$\langle\omega'|\omega\rangle = \delta(\omega'-\omega). \quad (7)$$

We factorize the projections (3) in a similar manner,

$$\begin{aligned}\Pi_{\rm E} &\simeq \sum_n |2n\rangle\langle 2n|\otimes\int_{-\Omega/2}^{\Omega/2} d\omega\, g(\omega)|\omega\rangle\langle\omega|, \\ \Pi_{\rm O} &\simeq \sum_n |2n+1\rangle\langle 2n+1|\otimes\int_{-\Omega/2}^{\Omega/2} d\omega\, g(\omega)|\omega\rangle\langle\omega|, \end{aligned} \quad (8)$$

where our requirement that $g(\omega)$ is negligible for $|\omega|>\Omega/2$ justifies restricting the integration over ω to the range

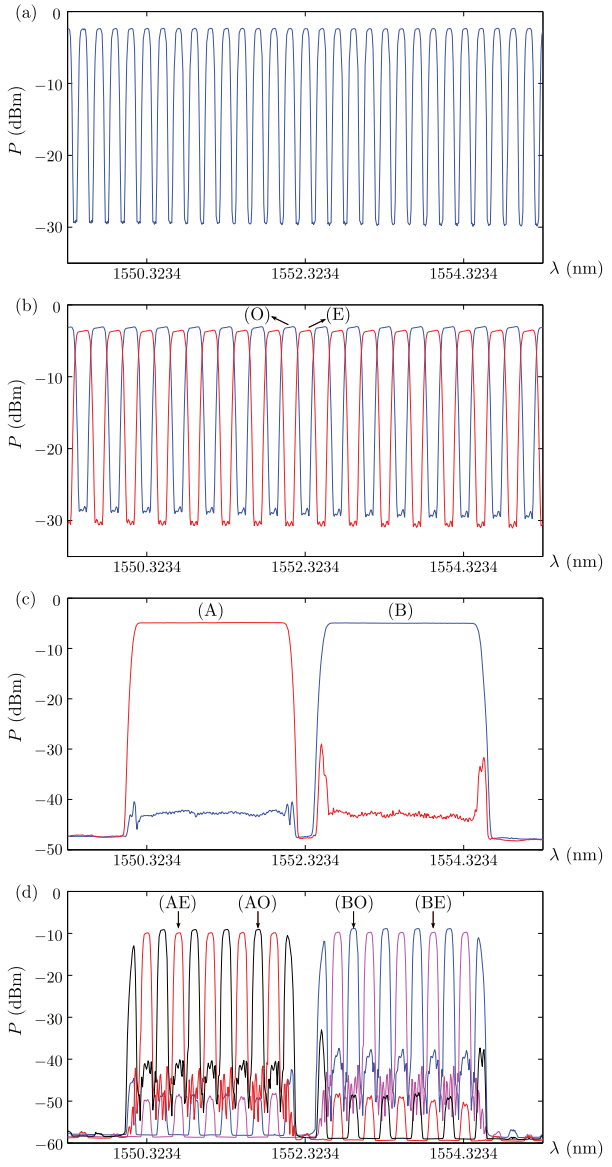

FIG. 2. (Color online) Spectrum of the filters used in the experiment. Since $\lambda_p = 776.1617$ nm, 1552.3234 nm corresponds to the degeneracy frequency ω_0. From top to bottom: (a) Output of the 12.5–25 interleaver. (b) Even (red [gray] curve labeled E) and odd (blue [gray] curve labeled O) outputs of a 25–50 interleaver. (c) Programmable WaveShaper filter; photons belonging to the red, labeled A (resp. blue, labeled B) output are sent to Alice (resp. Bob). (d) Spectrum obtained when cascading 12.5–25 interleaver, WaveShaper, and 25–50 interleaver; red (gray) curve labeled AE: Alice, even; black curve labeled AO: Alice, odd; magenta (gray) curve labeled BE: Bob, even; and blue (gray) curve labeled BO: Bob, odd. Note that whereas the outputs of the 25–50 interleavers [panel (b)] have ≈25 dB extinction at the center of each pass band, they only have ≈3 dB extinction at the edges of the band (where the red and blue curves cross). Hence photons at the edges of the pass bands have quite high and equal probabilities to exit the even and odd ports, which would result in an important decrease of visibility of interference if the 25–50 interleavers were used alone. The spectra in panel (d) show that upon using the initial 12.5–25 interleaver [depicted in panel (a)] that removes the photons at the edges of the pass bands, the even and odd outputs are now separated by 25 dB over the whole frequency band.

$[-\Omega/2,\Omega/2]$. Finally, in this representation, the action (2) of a phase modulator takes the expression

$$|n\rangle \otimes |\omega\rangle \mapsto \sum_{p\in\mathbb{Z}} J_p(c) e^{ip(\gamma-\pi/2)} |n+p\rangle \otimes |\omega\rangle = (U(c,\gamma)\otimes \mathbb{1}_{\text{off}})|n\rangle \otimes |\omega\rangle, \tag{9}$$

with the unitary transformation $U(c,\gamma)$ acting only on $\mathcal{H}_\Pi$, and $\mathbb{1}_{\text{off}}$ is the identity in the "offset" space.

We see explicitly, then, that the description of the relevant part of our setup is entirely contained in the discrete space $\mathcal{H}_\Pi$: Indeed, the offset frequency ω only affects the probability of response of the interleaver via the factor $|g(\omega)|^2$, and is otherwise never measured or recorded in the course of the experiment. Consequently, we restrict the remainder of the theoretical analysis to this space. Note that the factorization and isolation of the discrete space $\mathcal{H}_\Pi$ detailed here formalizes the concept of "frequency bin" previously used in Refs. [14,15].

B. Phase states and effective qubits

The effective qubits manipulated in our setup are made explicit when we express the source state $|\Psi_\Pi\rangle$ and actions of the phase modulators and interleavers in the basis of *even* and *odd phase states*. These states can be derived from our setup's symmetries with respect to translations of frequency bins. Formally, let us denote

$$\mathcal{T}_k : |n\rangle \mapsto |n+k\rangle \tag{10}$$

the (unitary) operation consisting of translation in the frequency domain by k frequency bins. The phase modulator and interleaver actions are symmetric with respect to translations by k and $2k$, respectively, in the sense that

$$[U(c,\gamma),\mathcal{T}_k] = 0, \quad k \in \mathbb{Z}, \tag{11}$$

and

$$[\Pi_{\text{E}},\mathcal{T}_k] = [\Pi_{\text{O}},\mathcal{T}_k] = 0, \quad k \in 2\mathbb{Z}, \tag{12}$$

while, using that the amplitude f_n varies slowly, the source state has the approximate symmetry

$$\mathcal{T}_k \otimes \mathcal{T}_{-k}|\Psi_\Pi\rangle \simeq |\Psi_\Pi\rangle. \tag{13}$$

Consequently, the phase modulators and source will share eigenstates with the $\mathcal{T}_1$ operator, while the interleaver action eigenstates will coincide with those of $\mathcal{T}_2$.

A full set of eigenstates of the $\mathcal{T}_1$ operator is given by the phase states, which we define by

$$|\varphi\rangle = \frac{1}{\sqrt{2\pi}} \sum_{n\in\mathbb{Z}} e^{in\varphi}|n\rangle, \tag{14}$$

such that $\mathcal{T}_k|\varphi\rangle = e^{-ik\varphi}|\varphi\rangle$. The inverse of this expression is given by

$$|n\rangle = \frac{1}{\sqrt{2\pi}} \int_{-\pi}^{\pi} d\varphi\, e^{-in\varphi}|\varphi\rangle. \tag{15}$$

For the $\mathcal{T}_2$ operator, a complete basis of eigenstates that will prove convenient is given by the even and odd phase

states

$$|\varphi\rangle_{\mathrm{E}} = \frac{1}{\sqrt{\pi}} \sum_{n\in 2\mathbb{Z}} e^{in\varphi}|n\rangle, \tag{16}$$

$$|\varphi\rangle_{\mathrm{O}} = \frac{1}{\sqrt{\pi}} \sum_{n\in 2\mathbb{Z}+1} e^{in\varphi}|n\rangle, \tag{17}$$

with $\mathcal{T}_2|\varphi\rangle_{\mathrm{E}} = e^{-2i\varphi}|\varphi\rangle_{\mathrm{E}}$ and $\mathcal{T}_2|\varphi\rangle_{\mathrm{O}} = e^{-2i\varphi}|\varphi\rangle_{\mathrm{O}}$. Note that

$$\begin{aligned} |\varphi\rangle &= \frac{1}{\sqrt{2}}[|\varphi\rangle_{\mathrm{E}} + |\varphi\rangle_{\mathrm{O}}], \\ |\varphi+\pi\rangle &= \frac{1}{\sqrt{2}}[|\varphi\rangle_{\mathrm{E}} - |\varphi\rangle_{\mathrm{O}}]. \end{aligned} \tag{18}$$

In terms of these states, the even and odd projection operators (restricted to the discrete space) take the expressions

$$\Pi_{\mathrm{E}} = \int_0^{\pi} d\varphi |\varphi\rangle_{\mathrm{E}}\langle\varphi|_{\mathrm{E}}, \tag{19}$$

$$\Pi_{\mathrm{O}} = \int_0^{\pi} d\varphi |\varphi\rangle_{\mathrm{O}}\langle\varphi|_{\mathrm{O}}, \tag{20}$$

and the entangled source state can be rewritten

$$\begin{aligned} |\Psi_{\Pi}\rangle &\simeq \frac{1}{\sqrt{N}} \sum_n |n\rangle|-n\rangle = \frac{1}{\sqrt{N}} \int_{-\pi}^{\pi} d\varphi |\varphi\rangle|\varphi\rangle \\ &= \frac{1}{\sqrt{N}} \int_0^{\pi} d\varphi (|\varphi\rangle_{\mathrm{E}}|\varphi\rangle_{\mathrm{E}} + |\varphi\rangle_{\mathrm{O}}|\varphi\rangle_{\mathrm{O}}), \end{aligned} \tag{21}$$

where we idealize $|\Psi_{\Pi}\rangle$ as an infinite sum, and N is a normalization constant symbolically representing the number of frequency bins over which f_n is nonzero, and formally equal to $2\pi\delta(0)$ (see also the discussion of normalization in Ref. [14]). To obtain the second line, we used that

$$\sum_{n\in\mathbb{Z}} e^{in\theta} = 2\pi \sum_{k\in\mathbb{Z}} \delta(\theta - 2\pi k). \tag{22}$$

The action of a phase modulator on a phase state is found to be

$$\begin{aligned} U(c,\gamma)|\varphi\rangle &= \frac{1}{\sqrt{2\pi}} \sum_m e^{im\varphi} \sum_p J_p(c) e^{ip(\gamma-\pi/2)}|m+p\rangle \\ &= \sum_p J_p(c) e^{ip(\gamma-\varphi-\pi/2)} \frac{1}{\sqrt{2\pi}} \sum_n e^{in\varphi}|n\rangle \\ &= e^{-ic\cos(\gamma-\varphi)}|\varphi\rangle, \end{aligned} \tag{23}$$

where, to obtain the last line, we used a version of the Jacobi-Anger expansion [29]:

$$e^{-ic\cos(\theta)} = \sum_n J_n(c) e^{in(\theta-\pi/2)}. \tag{24}$$

Using Eqs. (18) and (23) we readily find

$$\begin{aligned} U(c,\gamma)|\varphi\rangle_{\mathrm{E}} &= \cos(\theta)|\varphi\rangle_{\mathrm{E}} - i\sin(\theta)|\varphi\rangle_{\mathrm{O}}, \\ U(c,\gamma)|\varphi\rangle_{\mathrm{O}} &= -i\sin(\theta)|\varphi\rangle_{\mathrm{E}} + \cos(\theta)|\varphi\rangle_{\mathrm{O}}, \end{aligned} \tag{25}$$

where we have set $\theta = c\cos(\gamma-\varphi)$. For a fixed phase φ, we see that, varying the modulation parameters c and γ, we can implement a σ_x rotation of any desired angle between the even and odd phase states.

The above construction thus shows how to define effective qubits $\{|\varphi\rangle_{\mathrm{E}}, |\varphi\rangle_{\mathrm{O}}\}$ in the frequency domain, and how phase modulators realize σ_x rotations on the effective qubits. However, the angle of the rotation depends on the phase φ of the effective qubit. This phase is not experimentally accessible. Since the entangled state Eq. (21) is given by an integral over φ, this will imply a modified interference pattern with reduced visibility. In the next section we quantify this and show that the proposed experiment allows violation of the CHSH inequality.

C. Two-photon interference pattern

Modulating each arm of our setup with the modulation parameters $A = (a,\alpha)$ and $B = (b,\beta)$ transforms the initial source state to

$$\begin{aligned} |\Psi_{AB}\rangle = \frac{1}{\sqrt{N}} \int_0^{\pi} d\varphi \{&\cos(\theta_A+\theta_B)|\phi_{\varphi}^+\rangle \\ &- i\sin(\theta_A+\theta_B)|\psi_{\varphi}^+\rangle\}, \end{aligned} \tag{26}$$

where we have set $\theta_A \equiv \theta_A(\varphi) = a\cos(\varphi-\alpha)$ and $\theta_B \equiv \theta_B(\varphi) = b\cos(\varphi-\beta)$, and

$$|\phi_{\varphi}^+\rangle = |\varphi\rangle_{\mathrm{E}}|\varphi\rangle_{\mathrm{E}} + |\varphi\rangle_{\mathrm{O}}|\varphi\rangle_{\mathrm{O}}, \tag{27}$$

$$|\psi_{\varphi}^+\rangle = |\varphi\rangle_{\mathrm{E}}|\varphi\rangle_{\mathrm{O}} + |\varphi\rangle_{\mathrm{O}}|\varphi\rangle_{\mathrm{E}}. \tag{28}$$

Via elementary trigonometric identities, we have

$$\theta_A(\varphi) + \theta_B(\varphi) = D\cos(\varphi-\Delta) \equiv \theta_{AB}(\varphi), \tag{29}$$

with

$$D^2 = a^2 + b^2 + 2ab\cos(\alpha-\beta) \tag{30}$$

and

$$\tan(\Delta) = \frac{a\sin(\alpha) + b\sin(\beta)}{a\cos(\alpha) + b\cos(\beta)}. \tag{31}$$

The probability of jointly detecting two photons in even frequency bins is then given by

$$\begin{aligned} P(\mathrm{E},\mathrm{E}) &= \langle\Psi_{AB}|\Pi_{\mathrm{E}}\otimes\Pi_{\mathrm{E}}|\Psi_{AB}\rangle \\ &= \frac{1}{N}\int_0^{\pi} d\varphi' \int_0^{\pi} d\varphi \cos(\theta_{AB}(\varphi'))\cos(\theta_{AB}(\varphi)) \\ &\quad \times \langle\varphi'|_{\mathrm{E}}\Pi_{\mathrm{E}}|\varphi\rangle_{\mathrm{E}}\langle\varphi'|_{\mathrm{E}}\Pi_{\mathrm{E}}|\varphi\rangle_{\mathrm{E}} \\ &= \frac{\delta(0)}{N}\int_0^{\pi} d\varphi \cos(\theta_{AB}(\varphi))^2 \\ &= \frac{1}{4} + \frac{1}{4\pi}\int_0^{\pi} d\varphi \cos(2D\cos(\varphi-\Delta)) \\ &= \frac{1}{4}[1 + J_0(2D)]. \end{aligned} \tag{32}$$

To reach the last line, we used the integral expression

$$J_0(x) = \frac{1}{\pi}\int_0^{\pi} dt \cos(x\sin(t)) \tag{33}$$

for the zeroth Bessel function of the first kind, and that the function $t \mapsto \cos(x\sin(t))$ is π-periodic in t. We similarly

find

$$P(\mathrm{O,O}) = \tfrac{1}{4}[1 + J_0(2D)] \tag{34}$$

and

$$P(\mathrm{E,O}) = P(\mathrm{O,E}) = \tfrac{1}{4}[1 - J_0(2D)]. \tag{35}$$

Note that $P(\mathrm{E,E})$ and $P(\mathrm{O,O})$ never vanish, whereas $P(\mathrm{E,O})$ and $P(\mathrm{O,E})$ vanish whenever $D = 0$, which occurs whenever $a = b$ and $\alpha - \beta = \pi$. Because of the average over φ, the interference pattern differs from the traditional sine-squared function.

D. Maximal violation of the CHSH inequality

The main result of our experiment consists of an estimation of the CHSH expression

$$S = E(A_0B_0) + E(A_0B_1) + E(A_1B_0) - E(A_1B_1), \tag{36}$$

where $A_i \equiv (a_i,\alpha_i)$ and $B_j \equiv (b_j,\beta_j)$ denote choices of modulation amplitudes and phases,

$$E(A_iB_j) = P_{ij}(\mathrm{E,E}) - P_{ij}(\mathrm{E,O}) - P_{ij}(\mathrm{O,E}) + P_{ij}(\mathrm{O,O}), \tag{37}$$

and, e.g., $P_{ij}(\mathrm{E,E})$ is the probability of detecting two photons of even parity following modulation with the parameters A_i and B_j. Using Eqs. (32), (34), and (35), the CHSH correlator is given by

$$S = J_0(2D_{00}) + J_0(2D_{01}) + J_0(2D_{10}) - J_0(2D_{11}) \tag{38}$$

with

$${D_{ij}}^2 = {a_i}^2 + {b_j}^2 + 2a_ib_j\cos(\alpha_i - \beta_j). \tag{39}$$

Following reasoning similar to that in Ref. [15], we find that S is maximized by choosing modulation amplitudes and phases in such a way that $D_{00} = D_{01} = D_{10} = D_{11}/3$. This is achieved with phases given by $\alpha_0 = \beta_0 = \gamma$ and $\alpha_1 = \beta_1 = \gamma + \pi$ for some γ, and modulation amplitudes satisfying $a_0 = b_0 = c$ and $a_1 = b_1 = 3c$. We take, for c, the value that maximizes

$$S(c) = 3J_0(4c) - J_0(12c), \tag{40}$$

which is readily found numerically. The optimal modulation amplitudes are found this way to be $a_0 = b_0 = 0.2318$ and $a_1 = b_1 = 0.6955$. With these parameters, the CHSH correlator attains a maximal theoretical value of $S = 2.566$, thereby demonstrating that even though the interference is not perfect, a significant violation of the CHSH inequality is possible in this experiment.

IV. EXPERIMENTAL SETUP

The details of our experimental setup are depicted in Fig. 3. It is composed of commercially available fiber-pigtailed and opto-electronic components and operates in the telecommunication C band.

A continuous laser (Sacher) with power $P \approx 0.7\,\mathrm{mW}$ and stabilized wavelength $\lambda_p = 776.1617\,\mathrm{nm}$ pumps a periodically poled lithium niobate waveguide (HC Photonics), generating the frequency-entangled state

$$|\Psi\rangle = \int d\omega\, f(\omega)|\omega_0 + \omega\rangle|\omega_0 - \omega\rangle, \tag{41}$$

where $\omega_0/2\pi = c/2\lambda_p = 193.125\,\mathrm{THz}$ and $f(\omega)$ characterizes the two-photon bandwidth (approximately 5 THz). In what follows, we relate frequencies to the International Telecommunication Union Dense Wavelength Division Multiplexing grid in the C band: Multiples of 50 GHz are said to be on the 50 grid, multiples of 25 GHz are on the 25 grid, and other frequencies are off the grid.

In order to create a nice frequency comb, the photons pass through a 12.5–25 frequency interleaver (Optoplex). The photons whose frequencies belong to few-GHz-wide intervals centered on the 25 grid are collected at the output, while those centered on intervals with a 12.5 GHz offset are thrown away with more than 25 dB extinction. The reason for using this first filter is explained in the caption of Fig. 2, where the transmission spectra of all filters used in the experiment are shown.

The state at the output of this periodic filter can be written as in Eq. (5):

$$|\Psi\rangle = \sum_{n\in\mathbb{Z}} f_n|n\rangle|-n\rangle \otimes \int_{-\Omega/2}^{\Omega/2} d\omega\, h(\omega)|\omega\rangle|-\omega\rangle, \tag{42}$$

where $\Omega = 25$ GHz and $h(\omega)$ is a function that represents the effect of the 12.5–25 frequency interleaver (it is maximal around $\omega = 0$ and tends rapidly to zero). The pump is rejected with more than 100 dB extinction when taking into account all filters preceding detection.

Photons then pass through a programmable filter (WaveShaper from Finisar), which is configured to direct photons from bins $n = +(\text{resp. } -)1,2,3,4,5,6$ to Alice (resp. Bob). Thus we obtain the state

$$|\Psi\rangle = \frac{1}{\sqrt{6}}\sum_{n=1}^{6} |n\rangle|-n\rangle \otimes \int_{-\Omega/2}^{\Omega/2} d\omega\, h(\omega)|\omega\rangle|-\omega\rangle, \tag{43}$$

where we omit the factors f_n on such a reduced bandwidth. The restriction to only 6 frequency bins is realized so that dispersion can be neglected. Otherwise, photons in different frequency bins accumulate different phase shifts during propagation through the optical fibers that deteriorate the two-photon interference pattern. The number of frequency bins could be increased if dispersion compensation were implemented. Note that limiting the number of frequency bins will decrease the visibility of the interference pattern.

On each arm, a polarization controller followed by a polarizer ensures that the polarization of the photons is aligned with the axis of an electro-optic phase modulator (EOspace) driven by an adjustable 25-GHz radio-frequency signal. The radio-frequency architecture shown in the inset of Fig. 3 allows the phase modulation of each photon by radio-frequency signals $a\cos(\Omega t - \alpha)$, $b\cos(\Omega t - \beta)$ with independently adjustable amplitude a,b and phase α,β.

Finally, the photons are directed to a 25–50 frequency interleaver. One output collects photons belonging to the 50 grid, i.e., frequency bins with n odd (result O), while the other collects photons remaining from the 25 grid, i.e., frequency bins with n even (result E).

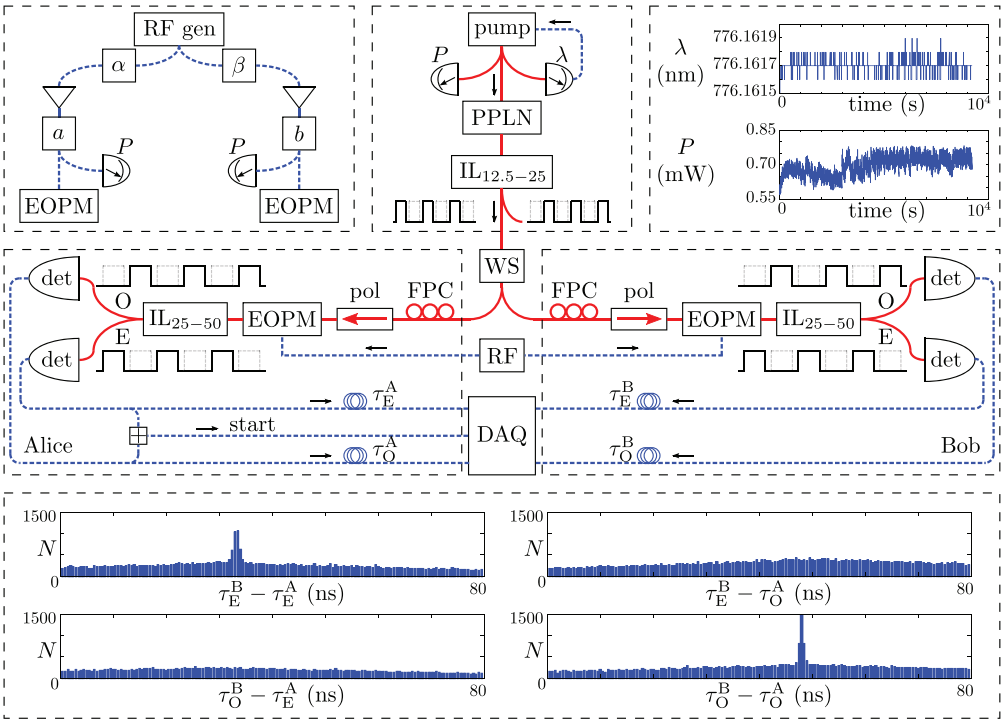

FIG. 3. (Color online) Experimental setup. Continuous red (gray) links are optical fibers and dashed blue (gray) links are electronic connections. A pump laser whose power P and wavelength λ are continuously monitored is directed through a periodically poled lithium niobate waveguide (PPLN). (Upper right: measurements of P and λ during the experiment; although P fluctuates, a retroaction loop acting on the piezoelectric element of the external cavity diode laser ensures that λ is constant.) Generated photon pairs pass through a 12.5- to 25-GHz interleaver ($\mathrm{IL}_{12.5-25}$) and a programmable filter (WS) which separates signal and idler photons, respectively, sent to Alice and Bob. On each arm, photons pass through a fiber polarization controller (FPC), a polarizer (pol), and an electro-optic phase modulator (EOPM) driven by a radio-frequency (rf) signal. (Upper left: schematic of the rf circuit. rf signals are generated by a 25-GHz rf generator whose power is split between Alice and Bob. On each arm, a variable phase shifter, an amplifier, and a variable attenuator ensure the precise adjustment of phase α,β and amplitude a,b, this last quantity being measured by a powermeter at the 10% output of a directional coupler placed before the EOPM. Isolators in the circuit (not shown) ensure that unwanted reflections do not distort the values of a,b,α,β.) After a 25- to 50-GHz interleaver (IL_{25-50}), single-photon detectors (det) record even (E) and odd (O) results. A data acquisition system (DAQ) registers detection coincidences and outputs histograms of these events. The DAQ is triggered by the arrival of a photon in one of Alice's detectors (start signal). The DAQ then records the exact time of arrival $\tau_{\mathrm{E,O}}^{\mathrm{A,B}}$ of photons coming from Alice's and Bob's detectors. (Bottom: typical results when no phase modulation is applied: one observes only EE and OO coincidences; with phase modulation, EO and OE coincidences would appear due to two-photon interference in the frequency domain.)

Four single-photon detectors (avalanche photodiodes id200 and id201 from idQuantique, efficiency 10%, repetition rate 100 kHz, gate width 100 ns, dark-count rates 0.2–0.6 kHz) allow the simultaneous acquisition of EE, EO, OE, and OO coincidences by a data acquisition system (Agilent Acqiris). Triggered by a detection on Alice's side, it registers the relative times between detections and outputs histograms of these events.

V. EXPERIMENTAL RESULTS

Histograms at the bottom of Fig. 3 correspond to coincidences in 0.5-ns steps measured during half an hour when no phase modulation was applied. One can see that only EE and OO coincidences are present, as expected by Eq. (43). We note that it is possible to change the correlations by changing the wavelength of the pump: e.g., when $\lambda_p = 776.1115\,\mathrm{nm}$, we measure inverted correlations.

Coincidences are measured at a rate of $\approx$1.5 Hz and with a coincidence-to-accidental ratio of $\approx$2. These low values are due to the high losses from pair creation to detection ($\approx$18 dB for each channel), and to the gated operation and high dark-count rates of the detectors used.

The experimental measurements, some of which are shown and discussed in Fig. 4, are in good agreement with the theoretical predictions, Eqs. (32), (34), and (35). When $a = b$, the probabilities $P(\mathrm{E,O})$ and $P(\mathrm{O,E})$ should vanish when the phase difference $\alpha - \beta$ is scanned, which enables one to define the visibility of the interference fringes as $V = (N_{\max} - N_{\min})/(N_{\max} + N_{\min})$, where $N_{\max,\min}$ are the net (dark counts subtracted) maximum and minimum number of counts per unit time. For the value $a = b = 0.6955$ used in the figure, we measure $V = 90\%$ and $V = 80\%$ depending on which combination, EO or OE, is considered. This limited visibility is attributed to nonideal state preparation: limited bandwidth and dispersion.

Finally, we demonstrate experimental violation of the CHSH Bell inequality Eq. (36). Experimentally, we evaluate

$$C_{ij} = \frac{N_{ij}^{-}}{N_{ij}^{+}}, \tag{44}$$

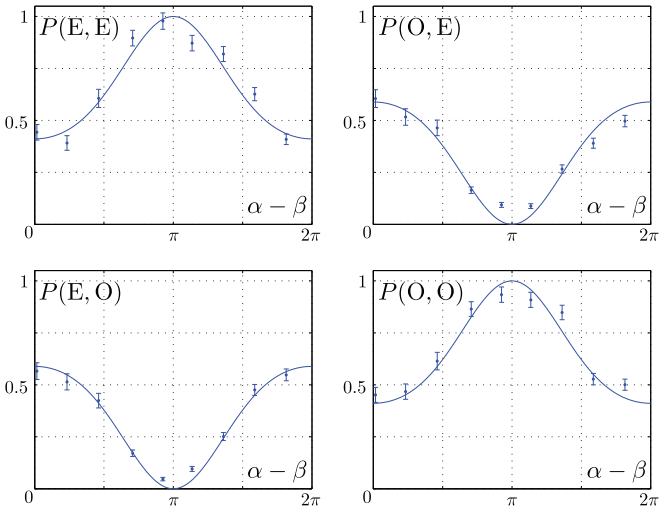

FIG. 4. (Color online) Two-dimensional two-photon interference patterns. Parameters are: $a = b = 0.6955$, and α is changed with β kept constant. Curves are theoretical predictions for coincidence probabilities P(E,E), P(E,O), P(O,E), and P(O,O); see Eqs. (32), (34), and (35). Symbols are experimental results: They correspond to the number of coincidences N(E,E), N(E,O), N(O,E), and N(O,O) simultaneously registered for each combination of outputs. Note that a normalization based on the coincidence rates registered when modulation is off is realized; error bars are statistical; background noise of the histograms has been subtracted. The net interference visibility (calculated on curves that should cancel) is evaluated to be $(85 \pm 5)\%$, depending on the combination considered.

with

$$N_{ij}^{\pm} \equiv N(\mathrm{E,E} \mid A_i, B_j) + N(\mathrm{O,O} \mid A_i, B_j) \pm [N(\mathrm{E,O} \mid A_i, B_j) + N(\mathrm{O,E} \mid A_i, B_j)], \quad (45)$$

from the number of coincidences N(E,E), N(E,O), N(O,E), and N(O,O) simultaneously registered for each combination of outputs, with parameters A_i and B_j deterministically and sequentially selected.

Our results are shown in Table I. One can see that the CHSH inequality is violated by more than 40 standard deviations. Although noise is subtracted, the theoretical optimum is not attained due to other experimental imperfections, mainly limited visibility.

TABLE I. CHSH Bell inequality violation. The first column corresponds to the optimal settings, $A_i = (a_i, \alpha_i)$, $B_j = (b_j, \beta_j)$, $i, j = 0, 1$, computed in Sec. III D. Second and third columns are theoretical predictions and experimental results, respectively.

	Theory	Experiment
A_0, B_0	0.796	0.764 ± 0.002
A_0, B_1	0.796	0.698 ± 0.002
A_1, B_0	0.796	0.714 ± 0.002
A_1, B_1	−0.178	-0.158 ± 0.002
S	2.566	2.334 ± 0.008

VI. CONCLUSION

In summary, we have demonstrated by two-photon interference and Bell inequality violation the manipulation of effective frequency qubits directly in the frequency domain at telecommunication wavelengths using standard telecommunication components. This further demonstrates the potential of frequency entanglement: One has the choice to exploit high-dimensional entanglement as in Refs. [14,15] or to manipulate more conventional two-dimensional entanglement, on which most quantum information protocols are based.

The reported experiment could be further improved. The coincidence rate, coincidence-to-accidental ratio, and interference visibility could be enhanced by the use of superconducting detectors. Using a designated filtering line and/or a source based on a resonator which would directly produce a frequency comb of the form Eq. (42) would limit losses and enhance purity of the quantum state. The full bandwidth of the two-photon state could be exploited provided dispersion management is realized. These improvements would bring the method demonstrated here closer to practical applications.

ACKNOWLEDGMENTS

This research was supported by the Interuniversity Attraction Poles program of the Belgian Science Policy Office, under Grant IAP P7-35 photonics@be, and by the F.R.S.-FNRS. E.W. acknowledges support from the Belgian Fonds pour la Formation à la Recherche dans l'Industrie et dans l'Agriculture (FRIA). The authors also thank the Conseil régional de Franche-Comté and the Partenariat Hubert Curien Tournesol.

[1] A. Aspect, P. Grangier, and G. Roger, Phys. Rev. Lett. **47**, 460 (1981).
[2] A. Aspect, P. Grangier, and G. Roger, Phys. Rev. Lett. **49**, 91 (1982).
[3] P. G. Kwiat, K. Mattle, H. Weinfurter, A. Zeilinger, A. V. Sergienko, and Y. Shih, Phys. Rev. Lett. **75**, 4337 (1995).
[4] J. G. Rarity and P. R. Tapster, Phys. Rev. Lett. **64**, 2495 (1990).
[5] A. Mair, A. Vaziri, G. Weihs, and A. Zeilinger, Nature (London) **412**, 313 (2001).
[6] J. Brendel, E. Mohler, and W. Martienssen, EPL (Europhys. Lett.) **20**, 575 (1992).
[7] P. G. Kwiat, A. M. Steinberg, and R. Y. Chiao, Phys. Rev. A **47**, R2472 (1993).
[8] P. D. Townsend, J. G. Rarity, and P. R. Tapster, Electron. Lett. **29**, 634 (1993).
[9] W. Tittel, J. Brendel, H. Zbinden, and N. Gisin, Phys. Rev. Lett. **81**, 3563 (1998).
[10] W. Tittel, J. Brendel, H. Zbinden, and N. Gisin, Phys. Rev. Lett. **84**, 4737 (2000).
[11] I. Marcikic, H. de Riedmatten, W. Tittel, H. Zbinden, M. Legré, and N. Gisin, Phys. Rev. Lett. **93**, 180502 (2004).

[12] J. D. Franson, Phys. Rev. Lett. **62**, 2205 (1989).
[13] A. K. Ekert, J. G. Rarity, P. R. Tapster, and G. Massimo Palma, Phys. Rev. Lett. **69**, 1293 (1992).
[14] L. Olislager, J. Cussey, A. T. Nguyen, P. Emplit, S. Massar, J.-M. Merolla, and K. Phan Huy, Phys. Rev. A **82**, 013804 (2010).
[15] L. Olislager, I. Mbodji, E. Woodhead, J. Cussey, L. Furfaro, P. Emplit, S. Massar, K. Phan Huy, and J.-M. Merolla, New J. Phys. **14**, 043015 (2012).
[16] J.-M. Merolla, Y. Mazurenko, J.-P. Goedgebuer, H. Porte, and W. T. Rhodes, Opt. Lett. **24**, 104 (1999).
[17] J.-M. Merolla, Y. Mazurenko, J.-P. Goedgebuer, and W. T. Rhodes, Phys. Rev. Lett. **82**, 1656 (1999).
[18] M. Bloch, S. W. McLaughlin, J.-M. Merolla, and F. Patois, Opt. Lett. **32**, 301 (2007).
[19] S. E. Harris, Phys. Rev. A, **78**, 021807(R) (2008).
[20] S. Sensarn, G. Y. Yin, and S. E. Harris, Phys. Rev. Lett. **103**, 163601 (2009).
[21] J. Capmany and C. R. Fernández-Pousa, JOSA B **27**, A119 (2010).
[22] C. H. Bennett and G. Brassard, in *Proceedings of IEEE International Conference on Computers, Systems and Signal Processing* (IEEE, New York, 1984), pp. 175–179.
[23] J. F. Clauser, M. A. Horne, A. Shimony, and R. A. Holt, Phys. Rev. Lett. **23**, 880 (1969).
[24] J. F. Clauser and M. A. Horne, Phys. Rev. D **10**, 526 (1974).
[25] M. A. Rowe, D. Kielpinski, V. Meyer, C. A. Sackett, W. M. Itano, C. Monroe, and D. J. Wineland, Nature **409**, 791 (2001).
[26] M. Ansmann, H. Wang, R. C. Bialczak, M. Hofheinz, E. Lucero, M. Neeley, A. D. O'Connell, D. Sank, M. Weides, J. Wenner, A. N. Cleland, and J. M. Martinis, Nature **461**, 504 (2009).
[27] A. Acín, N. Brunner, N. Gisin, S. Massar, S. Pironio, and V. Scarani, Phys. Rev. Lett. **98**, 230501 (2007).
[28] S. Pironio, A. Acín, S. Massar, A. Boyer de La Giroday, D. N. Matsukevich, P. Maunz, S. Olmschenk, D. Hayes, L. Luo, T. A. Manning, and C. Monroe, Nature **464**, 1021 (2010).
[29] A. Cuyt, V. Brevik Petersen, B. Verdonk, H. Waadeland, and W. B. Jones, *Handbook of Continued Fractions for Special Functions* (Springer, New York, 2008).